Acta Cryst. (1997). D53, 638–649

Comparison of Ternary Complexes of *Pneumocystis carinii* and Wild-Type Human Dihydrofolate Reductase with Coenzyme NADPH and a Novel Classical Antitumor Furo[2,3-*d*]pyrimidine Antifolate

VIVIAN CODY,[a]* NIKOLAI GALITSKY,[a] JOSEPH R. LUFT,[a] WALTER PANGBORN,[a] ALEEM GANGJEE,[b] RAJESH DEVRAJ,[b] SHERRY F. QUEENER[c] AND RAYMOND L. BLAKLEY[d]

[a]*Hauptman-Woodward Medical Research Institute, Inc., 73 High Street, Buffalo, NY 14203, USA,* [b]*Division of Medicinal Chemistry, Graduate School of Pharmaceutical Sciences, Duquesne University, Pittsburgh, PA 15282, USA,* [c]*Department of Pharmacology and Toxicology, Indiana University School of Medicine, Indianapolis, IN 46202, USA, and* [d]*Department of Molecular Pharmacology, St Jude Childrens Hospital, Memphis, TN 38105, USA.*
E-mail: cody@hwi.buffalo.edu

(*Received 4 October 1996; accepted 2 April 1997*)

Abstract

The novel furopyrimidine *N*-(4-{*N*-[(2,4-diaminofuro-[2,3-*d*]pyrimidin-5-yl)methyl]methylamino}benzoyl)-L-glutamate (MTXO), a classical antifolate with antitumor activity comparable to that of methotrexate (MTX), has been studied as inhibitor–cofactor ternary crystal complexes with wild-type *Pneumocystis carinii* (pc) and recombinant human wild-type dihydrofolate reductase (hDHFR). These structural data provide the first direct comparison of the binding interactions of the same antifolate inhibitor in the active site for pc and human DHFR. The human ternary DHFR complex crystallizes in the rhombohedral space group *R*3 and is isomorphous to the ternary complex reported for a γ-tetrazole methotrexate analogue, MTXT. The pcDHFR complex crystallizes in the monoclinic space group $P2_1$ and is isomorphous to that reported for a trimethoprim (TMP) complex. Interpretation of difference Fourier electron-density maps for these ternary complexes revealed that MTXO binds with its 2,4-diaminofuropyrimidine ring interacting with Glu32 in pc and Glu30 in human DHFR, as observed for MTXT. The presence of the 6–5 furopyrimidine ring instead of the 6–6 pteridine ring results in a different bridge conformation compared with that of MTXT. The bridge torsion angles for MTXO, *i.e.* C(4a)—C(5)—C(8)—N(9) and C(5)—C(8)—N(9)—C(1′), are −156.5/51.9° and −162.6/51.8°, respectively for h and pc, compared with −146.8/57.4° for MTXT. In each case, the *p*-aminobenzoylglutamate conformation is similar to that observed for MTXT. In the pcDHFR complex, the active-site region is conserved and the additional 20 residues in the sequence compared with the human enzyme are located in external loop regions. There is a significant change in the nicotinamide ribose conformation of the cofactor which places the nicotinamide O atom close to the $4NH_2$ group of MTXO (2.7 Å), a shift not observed in hDHFR structures. As a consequence of this, there is a loss of a hydrogen bond between the nicotinamide carbonyl group and the backbone of Ala12 in pcDHFR. In the human ternary complexes, the cofactor NADPH is bound with a more extended conformation, and the nicotinamide O atom makes a 3.5 Å contact with the $4NH_2$ group of MTXO. Although the novel classical antifolate MTXO is not highly active against pcDHFR, there are correlations between its binding interactions consistent with its lower potency as an inhibitor of h and pcDHFR compared with MTX.

1. Introduction

Dihydrofolate reductase (5,6,7,8-tetrahydrofolate:NADP oxidoreductase, E.C. 1.5.1.3, DHFR) catalyzes the reduction of 7,8-dihydrofolate to 5,6,7,8-tetrahydrofolate and is essential for the production of purine and pyrimidine precursors for RNA and DNA synthesis. For this reason it is a target for both antitumor and antimicrobial drug design (Blakley, 1995; Blakley & Benkovic, 1984; Kuyper *et al.*, 1996). More recently, antifolates have been shown to be effective against pneumonia from the fungal pathogen *Pneumocystis carinii* (pc), which is a major cause of mortality in patients with AIDS (Kovacs *et al.*, 1984, 1988; Allegra *et al.*, 1987). The current drug of choice for the treatment and prophylaxis of pc pneumonia is cotrimoxazole, which contains the antibacterial antifolate trimethoprim (TMP). Unfortunately, this drug is only modestly selective for pcDHFR. For example, the IC_{50} values of trimethoprim for *E. coli* (ec), human and pcDHFR are 2, 2000 and 20 000 n*M*, respectively. Methotrexate (MTX) is much more potent but is unselective, with IC_{50} values of about 0.1 n*M* for each enzyme (Edman *et al.*, 1989). The inhibitor dissociation constant (K_i) values for trimethoprim are 0.08, 196 and 152 n*M* in ec, h and pcDHFR, respectively (Margosiak, Appleman, Santi & Blakley, 1993).

Antifolates such as methotrexate require a specific active-transport system for cell entry which is present in

mammalian cells, but is absent in bacterial, fungal and protozoal cells. In order to bypass this system, antifolates with modified pteridine-ring structures and lipophilic side chains, such as trimetrexate (TMQ) and piritrexim (PTX), have been designed. These compounds enter cells by diffusion and have activity in some MTX-resistant cell lines and organisms (Allegra *et al.*, 1987; Kovacs *et al.*, 1988; Edman *et al.*, 1989). These lipophilic antifolates are also strong inhibitors of *P. carinii* DHFR, but they have only moderate selectivity (Kovacs *et al.*, 1988; Broughton & Queener, 1991). Thus, there is a need to develop antifolates which are strong inhibitors and have high selectivity for pcDHFR. The design of antifolates with increased pcDHFR selectivity is the target of several research groups (Gangjee, Shi, Queener, Barrows & Kisliuk, 1993; Piper *et al.*, 1993; Gangjee *et al.*, 1994; Then, Hartman & Kompis, 1993; Gangjee, Mavandadi, Queener & McGuire, 1995; Queener, 1995; Rosowsky *et al.*, 1995).

Crystallographic data have been reported for DHFR inhibitor complexes from several species (Champness *et al.*, 1994; Cody, Wojtczak, Kalman, Freisheim & Blakley, 1993; Cody *et al.*, 1992, 1995; Lewis *et al.*, 1995; Kraut & Matthews, 1987; Stammers *et al.*, 1987; Oefner, D'Arcy & Winkler, 1988) and reveal that the active-site characteristics are similar despite differences in their molecular size (*i.e.* bacterial 159–162, mammalian 186 and pc 206). All structures have an active site with the pteridine-ring binding pocket deep within a cavity lined by hydrophobic residues. In addition, there is a conserved acidic function (Glu30 in mammalian species) in the active site which forms an ionic interaction with the amino function of inhibitors, and a conserved arginine near the binding site entrance which forms an ionic interaction with the α-carboxyl group of folates. These data further show that the additional residues in the larger enzymes are insertions in regions that are loops between known secondary structural elements. Sequence alignment data reveal that pcDHFR contains those residues that are conserved in all DHFR enzymes and that the most significant changes in the active-site region involve substitution of phenylalanine at position 31 in human DHFR by isoleucine and asparagine 64 by phenylalanine (Edman *et al.*, 1989) (Fig. 1).

Although classical analogues do not penetrate *P. carinii* and *Toxoplasma gondii* (tg) organisms because they lack the folate transport mechanisms, classical analogues are of interest as molecular probes of the DHFR from these organisms. For example, the inhibitory potency of the novel furopyrimidine *N*-(4-{*N*-[(2,4-diaminofuro[2,3-*d*]pyrimidin-5-yl)methyl]methylamino}benzoyl)-L-glutamate (MTXO) and its N9-*des*-methyl analogue (Fig. 2) were evaluated against DHFR enzyme from pc, tg, rat liver (rl), *Lactobacillus casei* (lc), and human recombinant (h) sources (Gangjee *et al.*, 1994); these studies showed that both furopyrimidine analogues were significantly less potent against all DHFRs compared with MTX. It was observed that MTXO had a selectivity ratio of 6 against pcDHFR compared with hDHFR [selectivity ratio = IC_{50}(hDHFR)/IC_{50}(pcDHFR)], whereas MTX lacked significant selectivity against pcDHFR. Furopyrimidine analogues without the glutamate side chain had low inhibitory activity in

```
          Position

                1          7   10                  20  22              3031    3435
Human           V G S L N C I V A V S Q N M G I G K N G D L P W P P L R N E F R Y F Q R
pc      M N Q Q K S L T L I V A L T T S Y G I G R S N S L P W - K L K K E I S Y F K R
        1                 10                  20                  30

             40                        50                  60      64          70
Human   M T T T S S V E G K - - - Q N L V I M G K K T W F S I P E K N R P L K G R I N
pc      V T S F V P T F D S F E S M N V V L M G R K T W E S I P L Q F R P L K G R I N
         40                  50                  60                  70      75


                        80                  90                  100                 110
Human   L V L S R E L K E P P Q G A H F L S R S L D D A L K L T E Q P E L A N K V D -
pc      V V I T R N E S L D L G N G I H S A K S L D H A L E L L Y R T Y G S E S S V Q
           80                  90                  100                 110

                      117   120                 130                 140
Human   - - M V W I V G G S S V Y K E A M N H P G H L K L F V T R I M Q D F E S D T F
pc      I N R I F V I G G A Q L Y K A A M D H P K L D R I M A T I I Y K D I H C D V F
           120                 130                 140                 150

          150                                     160                         170
Human   F P E I D L E K Y K L - - - - - - - - - - L P E Y P G - - V L S D V Q E E K G
pc      F P L K F R D K E W S S V W K K E K H S D L E S W V G T K V P H G K I N E D G
              160                 170                 180                 190

                  180         186
Human   I K Y K F E V Y E K N D
pc      F D Y E F E M W T R D L
                  200         206
```

Fig. 1. Human DHFR sequence (186 residues) aligned with the sequence of *P. carinii* DHFR (206 residues) using the one-letter amino-acid code (Edman *et al.*, 1989). Key active-site residues are in bold type. Numbering above the sequence is for hDHFR and below for pcDHFR.

these assays (Gangjee *et al.*, 1994). One hypothesis for the lower activity was that the C(8)—N(9) bridge between the furopyrimidine and the substituted phenyl side chain is short by one C atom compared with MTX, because of the substitution at position 5 of the furo ring, which does not permit interaction with key residues in the DHFR active site. In order to understand the differences in activity of this series of furopyrimidine analogues and to assist in the design of analogues with increased pcDHFR inhibitory potency, we have determined the crystal structure of MTXO in complexes with NADPH from both pc and hDHFR.

2. Experimental methods

2.1. *Crystallization and X-ray data collection*

2.1.1. *P. carinii DHFR.* pcDHFR was isolated and purified by Queener (Broughton & Queener, 1991) and crystals of the 206-residue fungal enzyme with molecular weight 23 868 Da were grown using the hanging-drop vapor-diffusion method with silanized glass cover slips in a Z/3 plate (Luft *et al.*, 1994). The protein solution of pcDHFR was prepared in 0.1 *M* imidazole–HCl buffer (pH 7.0), and 1 m*M* dithiothreitol (DTT) incubated with NADPH, followed by addition of the inhibitor, MTXO. 5 µl protein droplets containing 3.6 mg ml^{-1} of pcDHFR in 10%(*w*/*v*) PEG 8K, 0.1 *M* imidazole–HCl buffer (pH 7.0), and 1 m*M* DTT, were suspended over a Z/3 gradient reservoir of length 73 mm, and solid NaCl (final concentration = 0.4 *M* based upon equivalent vapor-pressure experiments) overlaid with 0.1 *M* imidazole–HCl buffer (pH 7.0), 1 m*M* DTT, and 10%(*w*/*v*) PEG 8K. Crystals grew in three weeks. A small (0.75 × 0.25 × 0.15 mm) crystal was present in the Z/3 plate, which cracked on mounting. A fragment was moved away from the remaining piece and the crystal was screened for diffraction characteristics on a Rigaku R-AXIS imaging plate using a rotating-anode X-ray source.

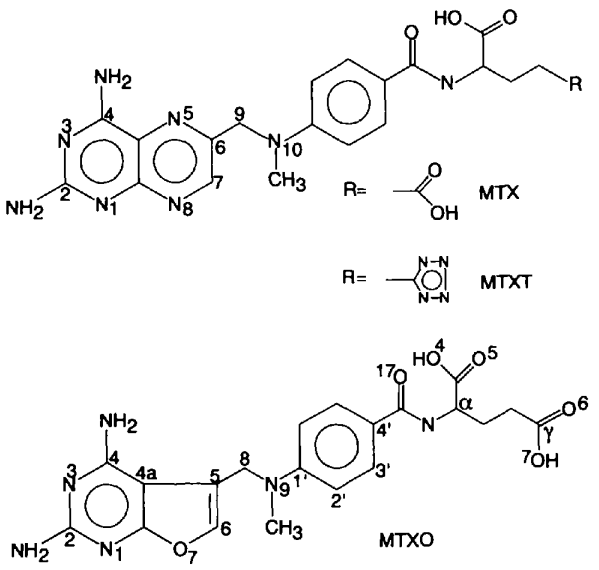

Fig. 2. Schematic diagram of the DHFR inhibitors MTX, MTXO and MTXT with numbering scheme.

The analysis of the diffraction data (Table 1) revealed that the crystal was monoclinic, of space group $P2_1$, with lattice constants $a = 37.17$ (6), $b = 43.09$ (4), $c = 61.05$ (8) Å and $\beta = 94.85$ (5)°. After post-refinement scaling, R_{merge} for the 2σ data was 6.66% for 5816 independent reflections to 2.3 Å resolution. There were 9177 reflections to 2.33 Å which were 67% complete between 2.5 and 2.4 Å with an F^2/σ ratio of 4.2, and 64% complete between 2.40 and 2.33 Å with an F^2/σ ratio of 3.9.

2.1.2. *Human DHFR.* Wild-type recombinant human DHFR was cloned, isolated and purified as described previously (Chunduru *et al.*, 1994). The protein was incubated in a molar excess of NADPH followed by the inhibitor, *N*-(4-{*N*-[(2,4-diaminofuro[2,3-*d*]pyrimidin-5-yl)methyl]methylamino}benzoyl)-L-glutamate (MTXO), which was synthesized as described previously (Gangjee *et al.*, 1994), and incubated overnight at 277 K. Hanging-drop experiments were carried out at 293 K with 62% ammonium sulfate, 0.1 *M* phosphate buffer (pH 8.0) in the wells and 3 µl protein solution mixed with 3 µl well solution in the droplet. Rhombohedral crystals grew in 2–4 weeks. Crystal lattice properties and data-collection statistics are listed in Table 1. Data collection was carried out on a Rigaku R-AXIS IIc imaging-plate system using a rotating-anode source. The crystal belongs to the space group *R*3 with hexagonal indexing.

2.2. *Structure determination and refinement*

2.2.1. *P. carinii DHFR.* Initially, molecular-replacement methods were used to phase the structure using the protein coordinates from the human DHFR structure (186 residues) as a starting model (Cody *et al.*, 1992). Rotation and translation searches were carried out using the program *X-PLOR* (Brünger, 1992). The Patterson correlation function was used to refine this search model. The best solution resulted in $R = 48.5\%$ for 3188 reflections between 10 and 4 Å resolution and was used to carry out the prep-stage refinement, using rigid-body restraints, for data between 8.0 and 2.6 Å resolution. This model resulted in $R = 31.0\%$. After simulated annealing and slow cooling from 3273 K, the model refined to 26.2% for data between 8.0 and 2.5 Å resolution.

Analysis of difference electron-density maps showed that the structure was conserved near the active-site region and that there was space in the structure for the several insertions in the 186 residues of the human structure compared with the 206 residues sequenced for pcDHFR (Edman *et al.*, 1989). The model from human DHFR was then mutated to the pc sequence and an 18-residue polyalanine sequence inserted for the missing sequence between residues Leu158 and Val165 in the

Table 1. *Refinement statistics for MTXO:NADPH:DHFR complexes*

	wt-h	pc
Lattice constants		
a (Å)	86.75	37.17
b (Å)		43.09
c (Å)	77.06	61.05
β (°)		94.9
Space group	*R*3	$P2_1$
Resolution range (Å)	8.0–2.10	8.0–2.3
No. of reflections used	10428	5631
R factor (%)	19.95	18.1
No. of protein atoms	1582	1686
No. of water molecules	35	42
B factor (protein average) (Å^2)	24.98	26.72

	Target *σ*	R.m.s. *σ*	
		wt-h	pc
Distances (Å)			
Bonds	0.020	0.027	0.012
Angles	0.040	0.066	0.038
Planar 1–4	0.050	0.070	0.033
Single torsion	0.500	0.243	0.213
Planar groups	0.020	0.019	0.010
Chiral volume	0.150	0.240	0.136
Multiple torsion	0.500	0.271	0.284
Possible hydrogen bonds	0.500	0.270	0.273
Torsion angles (°)			
Planar	5.0	3.1	1.8
Staggered	15.0	21.3	20.4
Orthonormal	15.0	21.6	27.3

human structure. After manual adjustment, this model was refined using the simulated-annealing and slow-cool protocols of *X-PLOR*. The resulting *R* was 23.2% for this model using data between 8.0 and 2.8 Å.

Inspection of the resulting difference electron-density map, using the program *CHAIN* (Sack, 1988) running on a Silicon Graphics Elan workstation, revealed appropriate density for the missing side chains of the polyalanine insertions and showed a reasonable fit for the flexible loop regions. Careful rebuilding of the model using a series of omit maps, particularly in the loop regions, was made before carrying out further refinement.

During the last stages of the *X-PLOR* refinement, coordinates for the pcDHFR ternary complex with trimethoprim (Champness *et al.*, 1994) became available from the Protein Data Bank (Reference code: 1DYR), and refinement of this structure was continued using coordinates from the 1.9 Å pcDHFR:TMP protein model. The improved phases resulted in a different interpretation for the flexible loop regions and better convergence of the refinement with an improved R_{free} compared with the previous model. Furthermore, there was good electron density for the cofactor and inhibitor, verifying that this structure is a ternary complex. The final cycles of refinement were carried out with the inhibitor and cofactor included using the program *PROLSQ* (Hendrickson & Konnert, 1980; Finzel, 1987; modified by G. D. Smith, HWI). The most poorly defined electron density in this structure was observed around residues 44–50, 82–91 and 110–114, which correspond to flexible loop regions. Similar density profiles were reported for pc TMP:NADPH and suggest that there is considerable flexibility in these regions (Champness *et al.*, 1994). Unlike the density reported for the TMP:pcDHFR structure, there is well defined electron density for the residues 41–44 in this structure. The Ramachandran conformational parameters from the last cycle of refinement (Fig. 3), generated by *PROCHECK* (Laskowski, MacArthur, Moss & Thornton, 1993) show that 84.3% of the residues have the most favored conformation and none is in a disallowed region.

2.2.2. *Human DHFR complex*. Since these human DHFR crystals are isomorphous with those of the wild-type human MTXT:NADPH ternary complex (Cody *et al.*, 1992), coordinates of the protein were used to calculate phases for this structure. Refinement was continued using the restrained least-squares program *PROLSQ* (Hendrickson & Konnert, 1980; Finzel, 1987; modified by G. D. Smith, HWI) in combination with the model-building program *CHAIN* (Sack, 1988). Initial refinement was begun using an overall *B* of 16 Å^2 for data between 8 and 3 Å, and was continued varying individual isotropic displacement parameters using the weighting scheme function $A + B\sin\theta/\lambda$, which varied *A* and *B*. The initial $(2|F_o| - |F_c|)\exp i\alpha_c$ maps, where F_o is the observed, F_c the calculated structure factor based on the protein model only, and α_c is the calculated phase, resulted in electron density corresponding to both the inhibitor MTXO and the reduced cofactor, NADPH, as well as a good fit of the protein to its density.

Further restrained refinement was continued for the ternary complex, including the cofactor and inhibitor

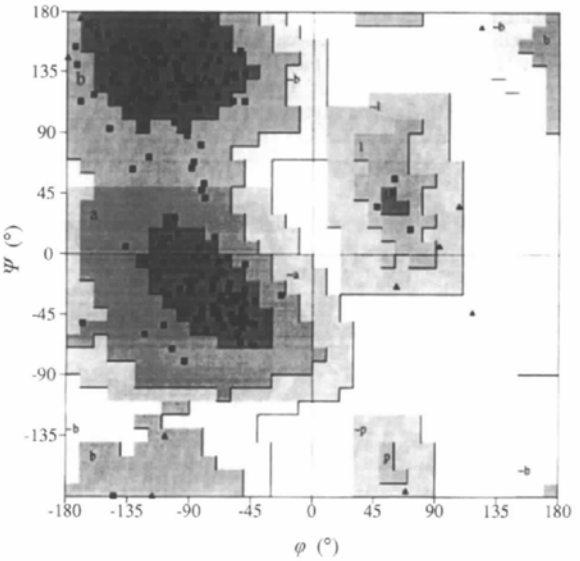

Fig. 3. Ramachandran plot for the pcDHFR ternary complex.

which were modeled on those of MTX, in which the pteridine ring was modified by using the builder function of *INSIGHTII* (Biosym Inc., 1995) (Fig. 2) and NADPH was taken from the wild-type ternary structure (Cody *et al.*, 1992). The aromatic rings of MTXO and NADPH were restrained to be planar. Between least-squares minimizations, the structures were manually adjusted to fit the electron-density values and verified by a series of omit maps calculated from the current model with deleted fragments. The highest displacement parameters (30–50 $Å^2$) of the protein residues are near the binding-site entrance and in flexible loop regions. The remaining side-chain displacement parameters range from 10 to 25 $Å^2$. In the final refinement stages, water molecules were added in accordance with the criteria of good electron density and acceptable hydrogen bonds to other atoms. The final refinement statistics are summarized in Table 1. Coordinates and structure factors for both structures have been deposited with the Protein Data Bank.†

3. Results

3.1. *Overall structure*

3.1.1. *pcDHFR*. The overall characteristics of the pcDHFR complex are similar to those reported for the trimethoprim complex (Champness *et al.*, 1994), and the active-site region is homologous to those of the mammalian and bacterial enzymes, re-emphasizing the conserved nature of the active site despite changes in enzyme size. As illustrated (Fig. 4), the orientation of the cofactor and inhibitor displays the same relative positions as observed in the human DHFR structures and the added 20 residues in pcDHFR compared with the human enzyme sequence are located in external loop regions.

Analysis of the primary sequence (Fig. 1) for pc and human DHFR reveals that, at neutral pH, the overall charge for the human enzyme is −1 and that for pcDHFR is +4. Comparison of the secondary structures of pc and human DHFR shows that many of the non-conserved sequence substitutions are located in regions where the topologies of the two enzymes differ, as observed between h residues 41–45 and pc 42–46, h 78–82 and pc 83–87, h 100–111 and pc 105–115, and between h 150–153 and pc 158–161. In other cases, a neutral or negative residue in the human enzyme is replaced by a positive one in pc. Many of these positive substitutions are located on the surface and interact with solvent. These changes are highlighted in a *GRASP* (Nicholls & Honig, 1991) representation of the molecular surfaces of the two enzymes (Fig. 5).

In a few instances, the replacement of a hydrophobic residue for a charged residue is a result of a twist in the backbone conformation of the pc structure, usually at an insertion point, such that the side chains lie on the opposite sides of the backbone. For example, Leu131 in the h structure is in a hydrophobic pocket surrounded by His127, Leu133, Leu4 and Ala6, whereas in the pc structure, the reversal of the backbone places the side chain of Asp139 toward the hydrophilic outside surface of the enzyme. A similar situation exists with h Arg136 and pc Ile145. As illustrated (Fig. 5), the effects of these sequence substitutions result in the pc enzyme being a more basic protein with an overall charge of +4. These changes could also affect the reaction rates of the two species, as observed from kinetic studies (Margosiak *et al.*, 1993).

The added three N-terminal residues of pcDHFR are near a flexible loop region between residues 102–107 in pc (97–105 for hDHFR). This region is highly flexible in all human structures, as indicated by their higher *B* values. A hydrogen-bond contact made between the backbone N atom of Lys5 and the hydroxyl group of Tyr106 in the pc structure stabilizes this region of the structure. This contact is not present in the human structure.

Analysis of the environment around Pro26 in the human structure reveals that the proline ring occupies a

† Atomic coordinates and structure factors have been deposited with the Protein Data Bank, Brookhaven National Laboratory, (Reference: 1DAJ, R1DAJSF). Free copies may be obtained through the Managing Editor, International Union of Crystallography, 5 Abbey Square, Chester CH1 2HU, England (Reference: GR0697).

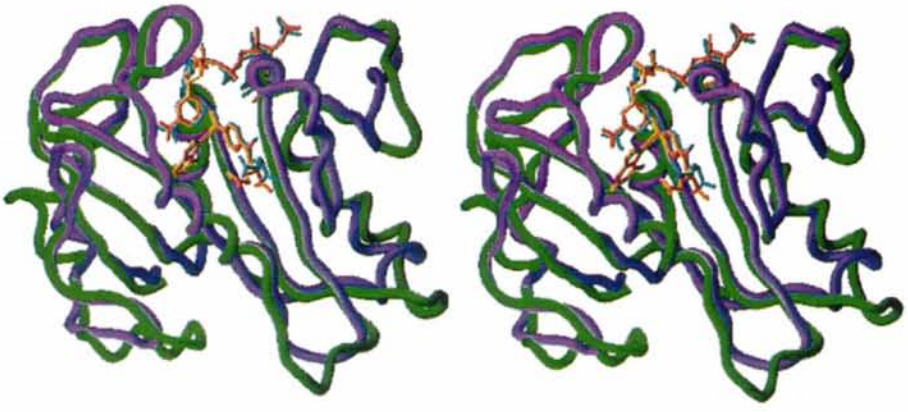

Fig. 4. Superposition of the backbone trace of the pcDHFR (green) ternary complex with MTXO and NADPH (cyan) on that of hDHFR (magenta) with the inhibitor complex (gold). The diagram was prepared using the program *SETOR* (Evans, 1993).

hydrophobic pocket made by the side chains of Phe142 and Leu175. In the pc structure, this pocket is made by the methylene C atoms of Lys28 and the residues Ile150 and Phe195. Similar conservation of function is revealed between the human residues Pro26 in which the carbonyl group forms a hydrogen bond to the amine group of Lys173. In pcDHFR, this contact is maintained by the carbonyl group of Lys28 and the side chain of Asp193, although there is a non-conserved change in the character of the residues.

There are three important sequence differences in the active site between pc and human DHFR (Fig. 1): phenylalanine 31 in the human enzyme is changed to isoleucine, asparagine 64 is changed to phenylalanine, and proline 25 is deleted and proline 26 is changed to lysine. The substitution of isoleucine at position 31 of hDHFR probably has little effect on binding affinity as the molar volume and hydrophobicity of these residues are similar. In bacterial DHFR, this position is occupied by leucine (Kraut & Matthews, 1987). The change at position 64 results in the loss of a hydrogen bond to a folate analogue. In the case of the smaller lipophilic antifolates such as piritrexim or trimethoprim there would be no effect. In the human enzyme, the prolines at

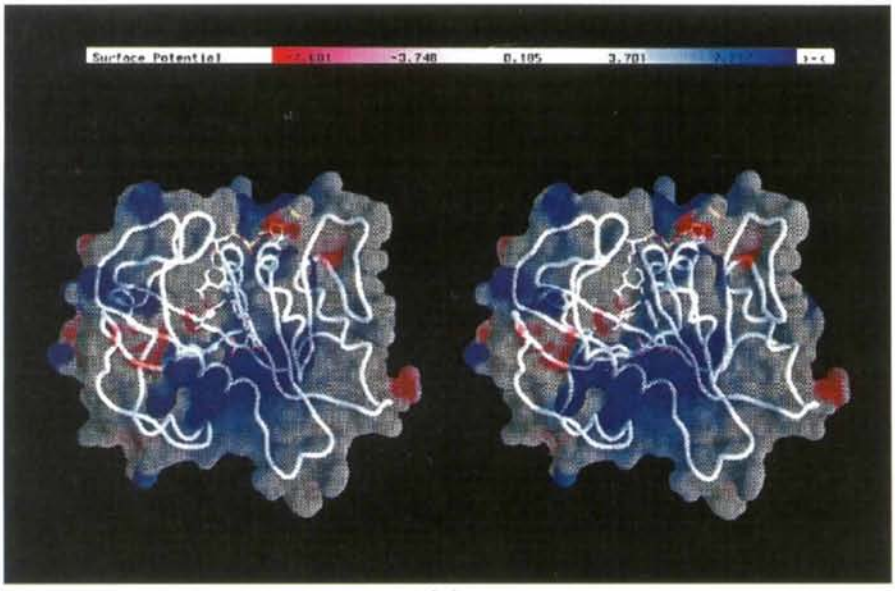

(*a*)

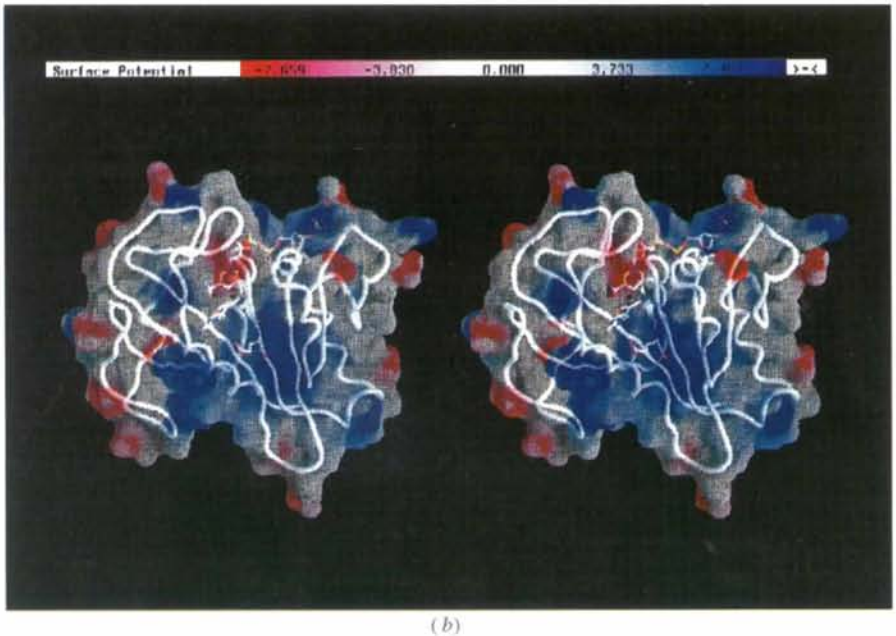

(*b*)

Fig. 5. (*a*) Solvent-accessible surface for the pcDHFR complex with MTXO and NADPH, calculated using *GRASP* (Nicholls & Honig, 1991). The positive regions (blue) and the negative regions (red) are highlighted on the surface. A superimposition of the worm representation of the protein backbone (white) and that atoms for MTXO and NADPH is shown. (*b*) Solvent-accessible surface for the hDHFR complex with MTXO and NADPH, calculated using *GRASP*. The positive regions (blue) and the negative regions (red) are highlighted on the surface. A superimposition of the worm representation of the protein backbone (white) and the atoms for MTXO and NADPH is shown.

positions 25 and 26 are involved in a tight turn, which is conserved in most DHFR structures. The combined deletion of Pro25 and change of Pro26 to Lys28 in pcDHFR results in a more flexible loop, although the side chain of the conserved tryptophan remains in the same location as observed in the human structures.

3.1.2. *Human DHFR.* The hDHFR:MTXO:NADPH ternary complex was compared with wt-hDHFR:MTXT:NADPH (Cody *et al.*, 1992) (Fig. 6). Least-squares superposition of all backbone atoms (*PROFIT* program; G. D. Smith, HWI library) showed that the root-mean-square (r.m.s.) deviation in the backbone positions in the MTXO complex was 0.17 Å from those in wt-hDHFR:MTXT:NADPH. There is also a *cis* peptide linkage between Arg65 and Pro66 and Gly116 and Gly117, as observed in other human DHFR complexes (Cody *et al.*, 1992, 1993).

3.1.3. *Inhibitor binding.* Fig. 7 shows the electron density from an $F_o - F_c$ omit map for MTXO in both pc and hDHFR. The density for the pc structure is less well defined, as indicated by the σ cut-off of the electron-density maps, than that observed for the human DHFR structure. The binding orientation of the furopyrimidine ring of MTXO is similar to that observed for the pteridine ring of methotrexate-bound human complexes (Cody *et al.*, 1992, 1993). As shown (Fig. 6, Table 2), the carboxylate O atoms of Glu30 protonate the furopyrimidine ring forming hydrogen bonds to N(1) by OE2 and OE1 to the N(2)-amino N atom. In addition, the carboxylate O atoms of the glutamate form hydrogen bonds to a conserved Thr and a structural water. The 2-amino group also hydrogen bonds to a structurally conserved water. In contrast, no structural water was observed near O(7), as is seen near N(8) of the pteridine antifolates (Cody *et al.*, 1992; Chunduru *et al.*, 1994). The glutamic acid residue, E32 in pcDHFR, maintains close contacts with the conserved Thr144, forming the tightly constrained polar pocket as observed in all other DHFR structures (Filman, Bolin, Matthews & Kraut, 1982).

The most interesting feature of the active-site interactions in this pcDHFR complex is the formation of a short contact between the 4-amino N atom of MTXO and the carboxamide O atom of NADPH (Fig. 8). This contact is not present in any of the human DHFR complexes nor in the structure of the pcDHFR:TMP complex (Champness *et al.*, 1994). This change is accompanied by the loss of the conserved hydrogen bond between the nicotinamide O atom and the backbone N atom of Ala12 (Table 2). Furthermore, there is an overall enhancement of the hydrogen-bonding interactions in the pcDHFR:MTXO complex caused by changes observed in the conformation of Tyr129. As illustrated (Table 2), these changes are not observed in either of the human DHFR complexes, nor in the structure of the pcDHFR:TMP:NADPH ternary complex. In the hDHFR ternary complex, the 4-amino group also forms intermolecular contacts with the backbone carbonyl group of Leu7, Val115, but is further away from the phenolic O atom of Tyr121 than observed in the hDHFR:MTXT:NADPH ternary complex (Table 2) (Cody *et al.*, 1992).

Because the geometry of the furopyrimidine differs significantly from that of pteridine, the furopyrimidine substituent at position 5 is oriented differently in the active site (Cody *et al.*, 1992). As shown (Fig. 6), this change places the C(8)—N(9) bridge of MTXO in a different orientation from that observed for C(9)—N(10) of MTXT. The bridge torsion angles for MTXO, *i.e.* C(4a)—C(5)—C(8)—N(9) and C(5)—C(8)—N(9)—C(1′), are −156.5/51.9° and −162.6/51.8°, respectively for h and pc, compared with −146.8/57.4° for MTXT. In each case, the *p*-aminobenzoylglutamate conformation is

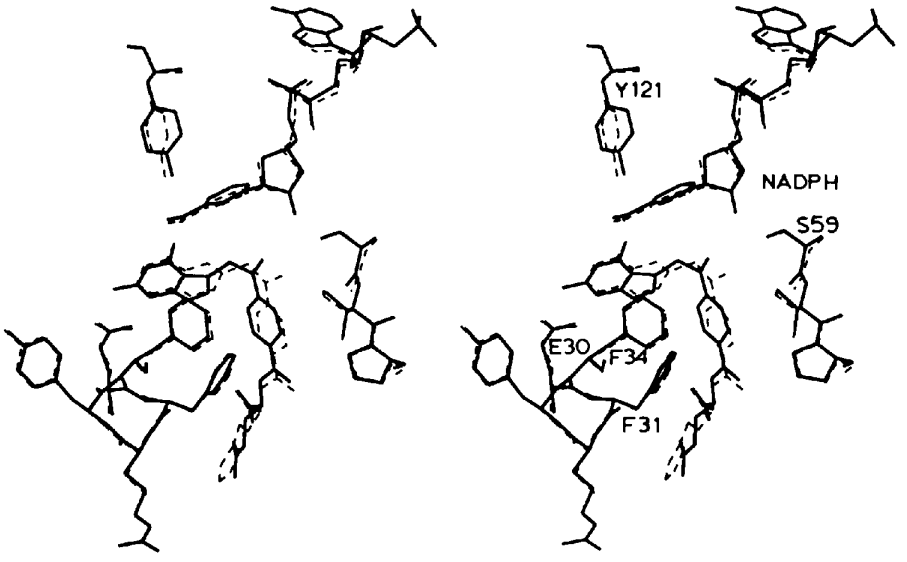

Fig. 6. Stereo superposition of the active-site region of human DHFR:NADPH inhibitor ternary complexes with MTXO (solid line) and MTXT (dashed line) (Cody *et al.*, 1992).

Table 2. *Summary of MTXO and NADPH:DHFR interactions (Å)*

A + or − superscript indicates addition or loss of a hydrogen bond in the pcDHFR:MTXO complex compared with human data.

	wt-hDHFR MTXO	wt-hDHFR MTXT†	pcDHFR MTXO	pcDHFR TMP‡
MTXO (h/pc)				
$4NH_2$···OH-Y121/Y129	3.7	3.6	3.4	3.6
$4NH_2$···O-Nic	3.5	3.5	2.7	3.8
$4NH_2$···O-V115/V123	3.4	3.1	2.7	2.9
$4NH_2$···O-I7 I10	3.1	3.1	3.1	2.9
$2\text{-}NH_2$···OE1-E30/E32	2.8	2.8	3.2	2.7
N1···OE2-E30/E32	2.7	2.8	2.6	2.8
OE2-E30/E32···Water	2.5	2.7	—	2.6
OE1-E30 E32···OγT136/T144	2.9	2.6	2.7	2.8
Oγ-T136 T144···Water	2.6	2.7	2.8	2.8
O17···N-N64 F69	2.9	2.8	—	—
O4···NH1-R70/R75	2.8	2.9	3.3	3.0/Water
O5···NH2-R70/R/75	2.3	2.6	3.5/2.6Water	3.4/Water
NADPH				
Nicotinamide carboxamide				
O···$4NH_2$MTXO	3.5	3.5	2.7'	3.8
O···N-A9 A12	2.9	3.0	3.6	3.0
O···OH-Y121 129	4.1	4.0	2.9'	3.7
N···O-A9 A12	2.8	2.6	2.8	2.8
N···O-I16 I19	3.2	3.2	3.2	2.9
O-I7 I10···OH-Y121/129	3.1	2.9	2.7	2.8
Nicotinamide ribose				
O1···Oγ-S59 S61	3.3	3.2	4.2	4.8
O2···Water	2.9	2.7	—	2.7
Pyrophosphate				
O5···N-S118 Q127	3.1	3.0	2.8	3.0
O15···N-T56/T61	2.7	2.7	3.0	3.0
O16···N-G117/G125	2.9	2.7	3.0	3.1
Adenine				
$5\text{-}NH_2$···Water	2.4	2.7	3.2	3.1
$5\text{-}NH_2$···OE2-E123	2.3	3.4	- -	—
2'-Phosphate				
O11···N-R77/R82	2.9	2.7	3.7	2.9
O12···Oγ-S76/S81	2.6	2.7	2.3	2.9
N_{nic}···$5\ NH_2$	17.5	18.0	16.4	16.5

† Cody *et al.* (1992). ‡ Champness *et al.* (1994).

similar to that observed for MTXT. The environment of the DHFR active site near the N-methyl of MTXO is primarily hydrophobic in nature, although there are some hydrophilic residues within the van der Waals sphere of the methyl group. The closest contacts observed for the N9-methyl of MTXO in hDHFR complexes are to the hydroxyl of Ser59 (3.5 Å), CD2 of Leu22 (3.7 Å), C5 of the nicotinamide ring of NADPH (4.1 Å), O1 of the nicotinamide ribose ring (3.9 Å), and to a water (4.2 Å), while in the pcDHFR:MTXO structure these contacts are to the backbone carbonyl group of Ser61 (4.9 Å), CD1 of Leu25 (4.3 Å) and C1 of the nicotinamide ring (4.1 Å). The corresponding contacts for the N10-methyl in MTXT of hDHFR (Cody *et al.*, 1992) are to the hydroxyl of Ser59 (3.6 Å), to CD1 of Leu22 (3.8 Å), to the nicotinamide ribose O1 (3.8 Å) and to a water (3.4 Å). The significant loss of potency of N9-*des*methyl MTXO indicates that it is important to fill this hydrophobic space. For example, in the structure of the ecDHFR ternary complex with folate and NADPH, there is a water molecule bound between the weaker binding folate 10-NH and the O^{γ} of Ser49 (Bystroff, Oatley & Kraut, 1990).

Close contacts of the antifolate γ-COOH with the conserved Arg (R70 and R75 for h and pcDHFR, respectively) constrain the *p*-aminobenzoyl-L-glutamate in its binding pocket. Thus, the greatest difference of this furopyrimidine binding conformation compared with MTX or MTXT is in the bridging group. However, in the pcDHFR:MTXO:NADPH ternary complex, the conformation of Phe69 is such that the phenyl ring is parallel to the glutamate methylene C atoms of MTXO, forming close hydrophobic contacts. The conformation of Phe69 in the ternary complex with trimethoprim differs as there are no inhibitor atoms in this region of the active site (Champness *et al.*, 1994).

3.1.4. *NADPH binding*. The coenzyme, NADPH, occupies a long shallow cleft that covers the carboxyl-terminal ends of five strands of β-sheet with the nicotinamide ring inserted between the carboxyl ends of two β-strands, βB (h 49–53/pc 54–58 for h and pcDHFR, respectively) and βE (h 112–116/pc 120–124). These two strands make tight turns into helices αF (h 54–59/pc 59–64) and αC (h 118–125/pc 126–133), respectively. As observed in other DHFR structures, the N-terminal positive ends of the helical dipoles are directed toward the center of the pyrophosphate segment of NADPH (Bystroff *et al.*, 1990; Cody *et al.*, 1992).

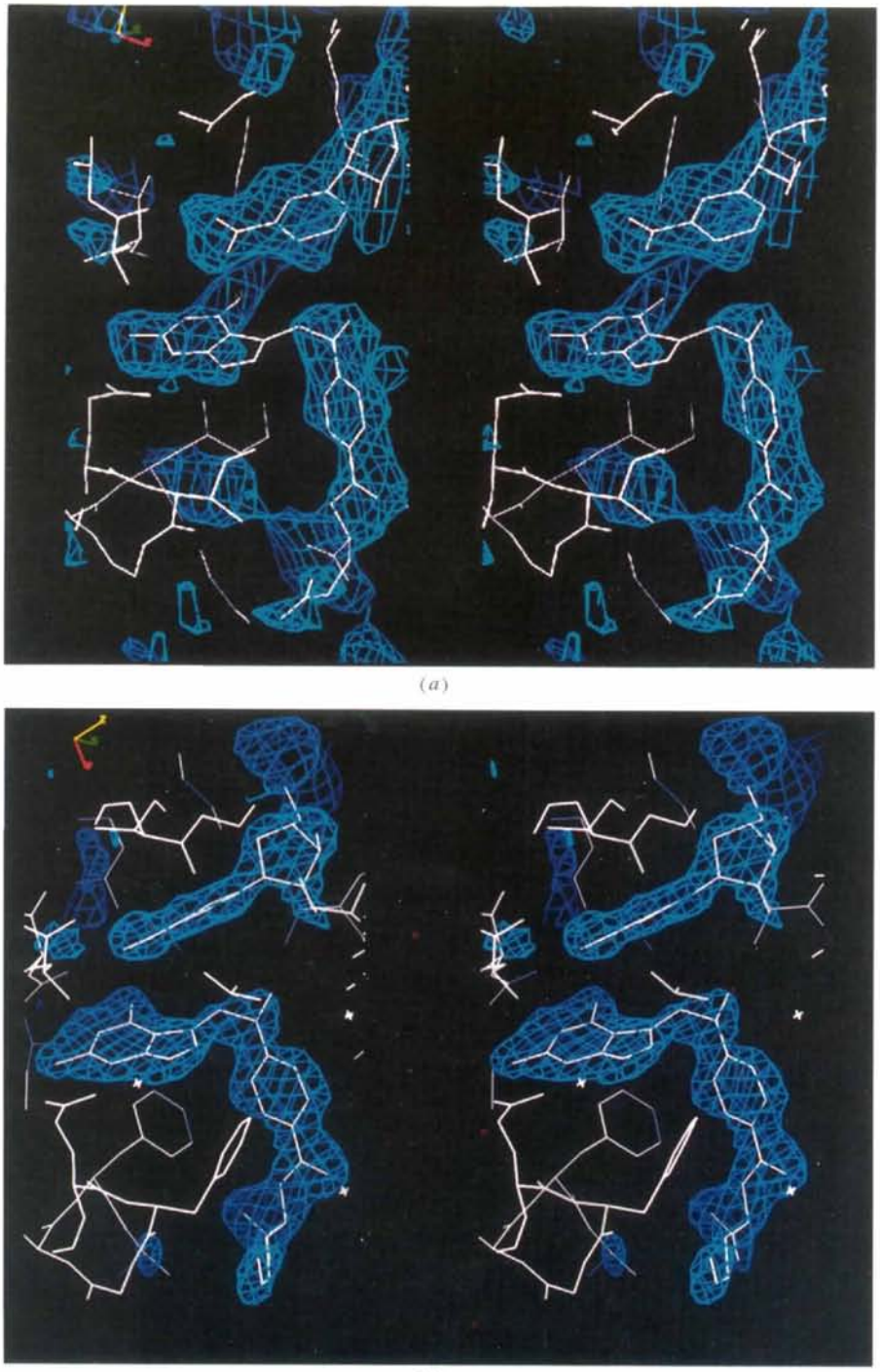

Fig. 7. (*a*) Stereo diagram of the $F_o - F_c$ omit map, contoured at 1σ, for MTXO in pcDHFR. (*b*) Stereo diagram of the $F_o - F_c$ omit map, contoured at 3σ, for MTXO in wt-hDHFR.

Although NADPH is bound in an extended conformation, similar to other cofactor complexes (Bolin, Filman, Matthews, Hamlin & Kraut, 1982; Filman *et al.*, 1982; Kraut & Matthews, 1987; Cody *et al.*, 1992, 1993), there is considerable variation in the conformation of the nicotinamide ribose moiety and the pyrophosphate moiety. The torsion angles ψ and φ specify the geometry of the pyrophosphate bridge and define the relationship between the two ribose moieties. The conformation of NADPH in the structure of the pcDHFR:MTXO:NADPH ternary complex shows the largest changes in conformation compared with other reported DHFR structures. In the hDHFR structure the torsion angle ψ (C10—O4—Pn—O7) is 10° while in the pc MTXO complex it is 38°, and in the pc TMP complex it is 75° (Champness *et al.*, 1994). The torsion angle φ_n (O4—Pn—O7—Pa) is similar for both the h and pc MTXO:DHFR complexes (118 and 115° for h and pc, respectively), but differs significantly from that observed in the pc TMP complex (68°). These changes reflect the overall conformational differences between h and pc DHFR and the consequences of specific inhibitor–enzyme interactions.

The distance between the adenosine ring amine and the nicotinamide amide has been used as a measure of the extension of the cofactor molecule (Rossmann, Liljas, Branden & Banaszak, 1975). As illustrated (Table 2), the cofactor is more extended in the hDHFR structures than in the pcDHFR complexes.

The carboxamide group of the nicotinamide ring, which is *syn* to the nicotinamide ring N atom, makes a series of strong hydrogen bonds to the conserved residues Ala9 and Ile16 in hDHFR (Ala12 and Ile19 for pcDHFR, Table 2). In addition, there are a series of non-bonded C—H···O contacts involving the nicotinamide ring C atoms and three neighboring O atoms of residues Leu7, Ile16 and Val115, which lie approximately in the plane of the nicotinamide ring. These features are conserved in all ternary complexes (Bolin *et al.*, 1982; Cody *et al.*, 1992).

Other cofactor–enzyme contacts include hydrogen bonds from the nicotinamide ribose hydroxyl (O2) to a structural water, from the pyrophosphate bridge O atoms to the backbone N atom of h Gly117 (G125), Thr56 (T61) and Ser118 (Q127), from the adenosine ribose 2′-phosphate O atoms to Ser76 (T81), Lys54 (R59) and Arg77 (R82). Similar contacts are made to the pc enzyme (Table 2).

The adenine ribose sugar adopts a C2′-*endo* conformation and C3′-*endo* conformation for the nicotinamide ribose. The bases are both *anti* ($\chi = \pm 100$–$135°$) with respect to the glycosidic linkage in all DHFR structures. The adenine ribose 2′-phosphate group fits into a pocket surrounded by charged or polar residues. The positively charged residue Lys54 in hDHFR is involved in potential electrostatic interactions to the negatively charged phosphate group. Contacts to Lys54, Ser76, Glu78 and the backbone of Arg77 in the human structures anchor the phosphate group, as do residues Arg59, Arg82 and Gln83 in pcDHFR. The binding of the pyrophosphate bridge region takes place between the amino ends of helices of the NADPH binding domain and close contacts are made to Gly116 and Gly117, which have a *cis* conformation. The other side of the adenine ring is in contact with the side chain of Lys55 of the human enzyme. Similar contacts are made in the pcDHFR structure.

4. Discussion

Structure–activity data for the inhibition of DHFR activity revealed that the novel classical furopyrimidine analogue, MTXO, was less potent than MTX in both human and *P. carinii* DHFR enzyme assays and further showed a significant loss of inhibitory potency for 9-*des*methyl MTXO, with a greater loss of activity in the pcDHFR assay (Gangjee *et al.*, 1994). Kinetic data measured for inhibitors of h and pcDHFR revealed comparable inhibitor dissociation (K_i) constants for MTX (Margosiak *et al.*, 1993) and tenfold weaker affinity for MTXO in these two enzyme systems (2.7 *versus* 6.5 n*M* for h and pc, respectively). However, caution should be used when correlating IC_{50} values with kinetic data as K_i depends on the concentration of dihydrofolate and of enzyme used in the assay. Nevertheless, these data are not necessarily inconsistent since the K_m value for dihydrofolate is 20 times higher for pcDHFR than for the human enzyme (Margosiak *et al.*, 1993; Blakley, 1995).

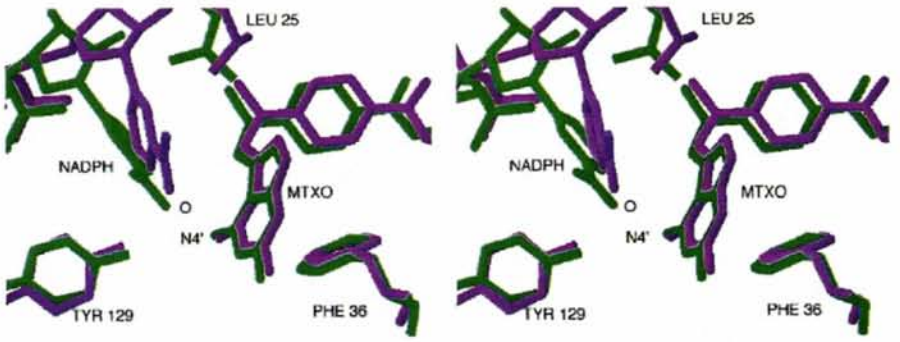

Fig. 8. Stereoview comparing the active-site geometry of the pcDHFR (green) MTXO:NADPH complex with that for the hDHFR (violet) complex. Note the conformational changes in the nicotinamide ribose ring, which result in a short O···N contact between the carboxamide O atom and $4NH_2$ of MTXO in pcDHFR (green).

This structural study provides the first opportunity to compare the molecular details of binding of the novel furopyrimidine classical antifolate MTXO to pcDHFR with its binding to hDHFR. This novel furopyrimidine antifolate binds to DHFR in an orientation similar to MTX, with the inhibitor N(1) and 2-NH_2 making close contacts to Glu30/Glu32 of the h and pcDHFR enzymes, respectively. Additionally, the furo ring O(7) of MTXO occupies the same position as observed for the 4-O of folic acid in the hDHFR: folate binary complex (Oefner *et al.*, 1988). Thus, in this binding mode, MTXO has substituents which probe both the 4NH_2 inhibitor and 4-O substrate sites. Additionally, the introduction of the furo ring system alters the conformation of the C(8)—N(9) bridge of MTXO compared with the C(9)—N(10) bridges of MTX and folate. This change results in weaker intermolecular contacts of the N(9) methyl and the surrounding environment of MTXO than observed for hDHFR complexes.

Comparison of the structural details between the h and pcDHFR:MTXO:NADPH complexes reveals a series of conformational changes which can be correlated to differences in binding affinity or inhibitory potency. The most significant differences between these pc and h enzyme complexes involve: (1) changes in the coenzyme nicotinamide ribose conformation in pcDHFR, which permit a short contact between the nicotinamide carboxamide O atom and 4NH_2 group of MTXO and which is not observed in either the h ternary complex or in the pcDHFR:NADPH:TMP structure, (2) a change in the conformation of Tyr129, which results in a hydrogen-bond contact to the 4NH_2 group of MTXO in the pcDHFR complex, also not observed in the hDHFR:MTXO:NADPH complex, and (3) a change in the conformation of Phe69 of pcDHFR:MTXO:NADPH, which enhances the hydrophobic contacts between the γ-glutamate methylene C atoms of MTXO, contacts not possible in the human enzyme complex as Phe69 is replaced by Asn64 in the human enzyme, which makes a hydrogen-bond contact to the carbonyl O17 of MTXO. Additionally, changes in the hydrophobicity of the active site as a result of sequence changes between the two enzyme classes will also influence binding affinity and inhibitory potency. Structural data for the pcDHFR:TMP:NADPH ternary complex (Champness *et al.*, 1994) show that the conformational changes in the nicotinamide ribose moiety are intermediate between those observed in these pc MTXO and h MTXO enzyme complexes, and show no short contact between the nicotinamide carboxamide and the 4NH_2 group of TMP. Furthermore, because there are no inhibitor interactions in the glutamate binding pocket, the conformation of Phe69 in the TMP complex is different from that of the pcDHFR:MTXO complex.

An explanation for the large decrease in IC_{50} of MTXO for hDHFR compared with MTX, and the similar decrease for pcDHFR, is less obvious from these structural data and lies in contributions from changes in the N-methyl bridge conformation between MTXO and MTX. The sensitivity of the environment around the N-methyl is further highlighted by the significant loss of inhibitory potency for 9-*des*methyl MTXO compared with MTXO, in particular for the pcDHFR enzyme (Gangjee *et al.*, 1994). Although there is a shift in the placement of the N-methyl bridge in the MTXT structure of the human complex (Cody *et al.*, 1992) (Fig. 6), the intermolecular contacts are similar to those of MTXO. Comparison of the intermolecular contacts to the N-methyl of MTXO reveal that small rearrangements in the pcDHFR:MTXO:NADPH structure weaken all the contacts compared with those found in the hDHFR:MTXO:NADPH complex. One of the major changes in conformation in this region of the active site is the conformation of Ser59 in the human enzyme and its corresponding Ser64 in pcDHFR. In the human MTXO complex, the O^{γ} S59 is oriented toward the N-methyl group and participates in two hydrogen bonds with the carbonyl O atom of Thr56 and with the hydroxyl group of the nicotinamide ribose ring. In the pc structures (including that of the pc TMP complex), the O^{γ} S64 is oriented away from MTXO and forms hydrogen bonds to the carbonyl group of Gln23 and the carbonyl group of Lys60. Because of the conformational change in NADPH, the cofactor no longer comes within hydrogen-bonding contact distance to Ser64. These changes could be influenced by differences in the loop conformation between residues 16–21 in hDHFR and 19–24 in pcDHFR. In the human structures, Lys55 interacts with a water molecule, whereas in the pcDHFR structure, the corresponding Lys60 forms a hydrogen bond to Gln23. Gly20 is also within van der Waals contact distance to the ribose of NADPH in human DHFR, but Gln23 of pcDHFR does not form such contacts. Therefore, the interplay of these residues may contribute to the binding affinity of the antifolates.

Other contributions to the differences in inhibitory potency of MTXO and MTX are interactions with the furan ring. There is a conserved structural water molecule present in the reported crystal structures of bacterial and human DHFR:MTX:NADPH ternary complexes which interacts with N8 of MTX (Kraut & Matthews, 1987; Cody *et al.*, 1992). There are no close interactions with the furo O atom of MTXO in either the h or pcDHFR ternary complexes. In addition, the effects of the furo substituent on the basicity of the pyrimidine ring may also influence MTXO binding affinity. These differences could be exploited in inhibitor design to increase the selectivity of antifolates for pcDHFR.

In summary, these data allow the first direct comparison of the binding interactions of a single antifolate to both human and *P. carinii* dihydrofolate reductase and reveal a series of conformational changes near the active site of pcDHFR, which exploits differences in sequence and lipophilic properties of the residues between species.

Although the novel classical furopyrimidine MTXO is not highly active against pcDHFR, there are correlations between the binding interactions consistent with its lower potency as an inhibitor of h and pc DHFR compared with MTX. These data provide a platform from which to consider further drug design experiments to obtain more pc-selective antifolates.

This work was supported in part by: CA-31922, CA-21765 and American Lebanese Syrian Associated Charities (RLB); GM-40998 and AI-30900 (AG); AmFAR 02135-15RG, GM-51670 and the Buffalo Foundation (VC). VC also thanks Dave Pawlowski for crystal growth experiments.

References

Allegra, C. J., Kovacs, J. A., Drake, J. C., Swan, J. C., Chabner, B. A. & Masur, H. (1987). *J. Exp. Med.* **164**, 926–931.

Biosym Inc. (1995). *INSIGHTII*, Biosym Inc., Molecular Simulations, Inc., San Diego, CA.

Blakley, R. L. (1995). *Eukaryotic Dihydrofolate Reductase.* In *Advances in Enzymology and Related Areas of Molecular Biology*, Vol. 70, edited by A. Meister, pp. 23–102. New York: John Wiley.

Blakley, R. L. & Benkovic, S. J. (1984). *Folates & Pteridines*, Vol. 1. New York: John Wiley.

Bolin, J. T., Filman, S. J., Matthews, D. A., Hamlin, R. C. & Kraut, J. (1982). *J. Biol. Chem.* **257**, 13650–13662.

Broughton, M. C. & Queener, S. F. (1991). *Antimicrob. Agents Chemother.* **35**, 1348–1355.

Brünger, A. T. (1992). *X-PLOR.* Yale University Press.

Bystroff, C., Oatley, S. J. & Kraut, J. (1990). *Biochemistry*, **29**, 3263–3277.

Champness, J. N., Achari, A., Ballantine, S. P., Bryant, P. K., Delves, C. J. & Stammers, D. K. (1994). *Structure*, **2**, 915–924.

Chunduru, S. K., Cody, V., Luft, J. R., Pangborn, W., Appleman, J. R. & Blakley, R. L. (1994). *J. Biol. Chem.* **269**, 9547–9555.

Cody, V., Galitsky, N., Luft, J. R., Pangborn, W., Gangjee, A., Bolyard, L. & Queener, S. F. (1995). *Proc. Am. Assoc. Cancer Res.* **36**, 407.

Cody, V., Luft, J. R., Ciszak, E., Kalman, T. I. & Freisheim, J. H. (1992). *Anticancer Drug Design*, **7**, 483–491.

Cody, V., Wojtczak, A., Kalman, T. I., Freisheim, J. H. & Blakley, R. L. (1993). *Conformational Analysis of Human Dihydrofolate Reductase Inhibitor Complexes: Crystal Structure Determination of Wild Type and F31 Mutant Binary and Ternary Inhibitor Complexes.* In *Chemistry and Biology of Pteridines and Folates*, edited by J. E. Ayling, M. G. Nair & C. M. Baugh, pp. 481–486. New York: Plenum Press.

Edman, J. C., Edman, U., Cao, M., Lundgren, B., Kovacs, J. A. & Santi, D. V. (1989). *Proc. Natl Acad. Sci. USA*, **86**, 8625–8629.

Evans, S. V. (1993). *J. Mol. Graph.* **11**, 148–153.

Filman, D. S., Bolin, J. T., Matthews, D. A. & Kraut, J. (1982). *J. Biol. Chem.* **257**, 13663–136672.

Finzel, B. C. (1987). *J. Appl. Cryst.* **20**, 53.

Gangjee, A., Devraj, R., McGuire, J. J., Kisliuk, R. L., Queener, S. F. & Barrows, L. R. (1994). *J. Med. Chem.* **37**, 1169–1176.

Gangjee, A., Mavandadi, F., Queener, S. F., McGuire, J. J. (1995). *J. Med. Chem.* **38**, 2158–2165.

Gangjee, A., Shi, J., Queener, S. F., Barrows, L. R. & Kisliuk, R. L. (1993). *J. Med. Chem.* **36**, 3437–3443.

Hendrickson, W. A. & Konnert, J. H. (1980). *Computing in Crystallography*, edited by R. Diamond, S. Ramaseshan & K. Venkatesan, p. 13.01. Bangalore: Indian Academy of Sciences.

Kovacs, J. A., Allegra, C. J., Swan, J. C., Drake, J. C., Parrillo, J. E., Chabner, B. A. & Masur, H. (1988). *Antimicrob. Agents Chemother.* **32**, 430–433.

Kovacs, J. A., Hiemenz, J. R., Macher, A. M., Stover, D., Murray, H. W., Shellhamer, J., Lane, H. C., Urmacher, C., Honig, C., Longo, D. L., Parker, M. M., Natanson, C., Parrillo, J. E., Fauci, A. S., Pizzo, P. A. & Masur, H. (1984). *Ann. Intern. Med.* **100**, 663–671.

Kraut, J. & Matthews, D. A. (1987). *Dihydrofolate Reductase.* In *Biological Macromolecules and Assemblies*, Vol. III, edited by F. Jurnak & A. McPherson, pp. 1–71. New York: John Wiley.

Kuyper, L. F., Baccanari, D. P., Jones, M. L., Hunter, R. N., Tansik, R. L., Joyner, S. S., Boyton, C. M., Rudolph, S. K., Knick, V., Wilson, H. R., Caddell, J. M., Freidman, H. S., Comley, J. C. & Stables, J. N. (1996). *J. Med. Chem.* **39**, 892–903.

Laskowski, R. A., MacArthur, M. W., Moss, D. S. & Thornton, J. M. (1993). *J. Appl. Cryst.* **26**, 283–291.

Lewis, W. S., Cody, V., Galitsky, N., Luft, J. R., Pangborn, W., Chunduru, S. K., Spencer, H. T., Applemann, J. R. & Blakley, R. L. (1995). *J. Biol. Chem.* **270**, 5057–5064.

Luft, J. R., Arakali, S. V., Kirisits, M. J., Kalenik, J., Wawrzak, I., Cody, V. & DeTitta, G. T. (1994). *J. Appl. Cryst.* **27**, 443–452.

Margosiak, S. A., Appleman, J. R., Santi, D. V. & Blakley, R. L. (1993). *Arch. Biochem. Biophys.* **305**, 499–508.

Nicholls, A. & Honig, B. (1991). *GRASP.* Columbia University, USA.

Oefner, C., D'Arcy, A. & Winkler, F. K. (1988). *Eur. J. Biochem.* **174**, 377–385.

Piper, J. R., Johnson, C. A., Hosmer, C. A., Carter, R. L., Pfefferkorn, E. R., Borotz, S. E. & Queener, S. F. (1993). *Lipophilic Antifolates as Candidates Against Opportunistic Infections.* In *Chemistry and Biology of Pteridines and Folates*, edited by J. E. Ayling, M. G. Nair & C. M. Baugh, pp. 429–433. New York: Plenum Press.

Queener, S. F. (1995). *J. Med. Chem.* **38**, 4739–4759.

Rosowsky, A., Mota, C. E., Queener, S. F., Waltham, M., Ercikan-Abali, E. & Bertino, J. R. (1995). *J. Med. Chem.* **38**, 745–752.

Rossmann, M. G., Liljas, A., Branden, C. I. & Banaszak, L. J. (1975). *Enzymes*, **11**, 61–102.

Sack, J. S. (1988). *J. Mol. Graph.* **6**, 224–225.

Stammers, D. K., Champness, J. N., Beddell, C. R., Dann, J. G., Eliopoulos, E., Geddes, A., Ogg, D. & North, A. C. T. (1987). *FEBS Lett.* **218**, 178–182.

Then, R. L., Hartman, P. G. & Kompis, I. (1993). *Selective Inhibition of DHFR from Problem Human Pathogens.* In *Chemistry and Biology of Pteridines and Folates*, edited by J. E. Ayling, M. G. Nair & C. M. Baugh, pp. 533–537. New York: Plenum Press.